Möbius Registration

Alex Baden¹, Keenan Crane², and Misha Kazhdan¹

¹Johns Hopkins University ²Carnegie Mellon University

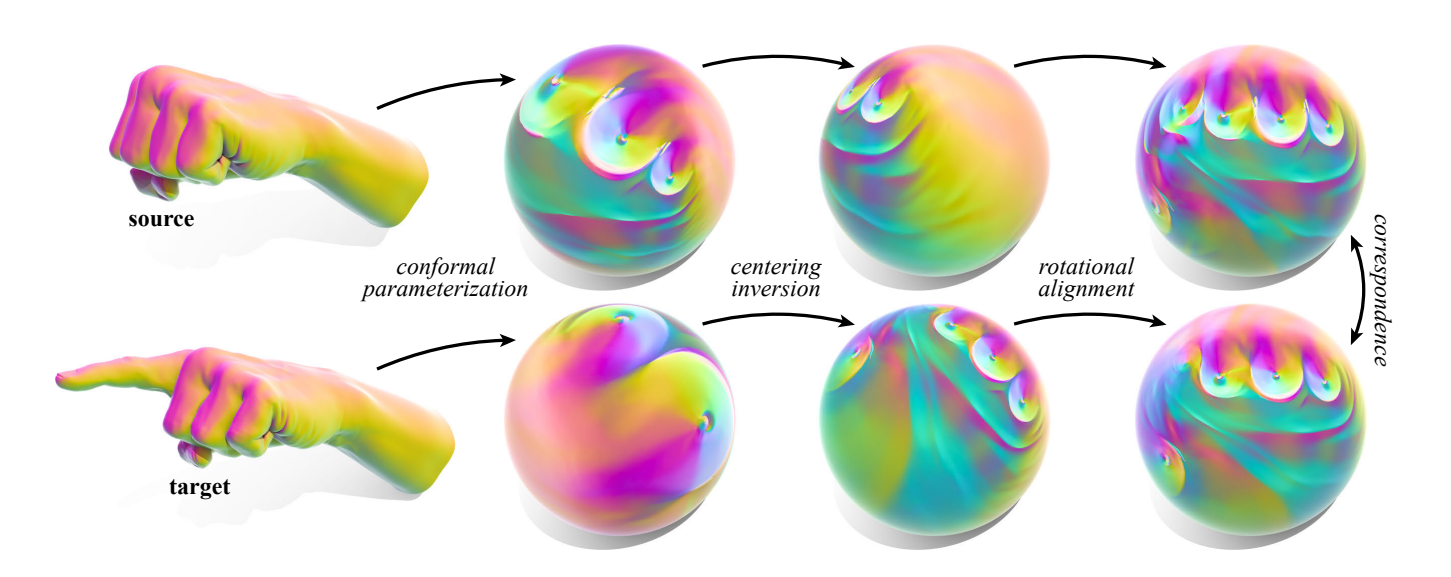


Figure 1: Even for near-isometric surfaces, correspondence problems can be quite challenging. Here we first compute a conformal parameterization over the sphere (left). Since this parameterization is not unique, we must pick an inversion (center) and rotation (right) that best registers the two maps. We describe a fast, simple procedure for computing this transformation, and generalizations thereof.

Abstract

Conformal parameterizations over the sphere provide high-quality maps between genus zero surfaces, and are essential for applications such as data transfer and comparative shape analysis. However, such maps are not unique: to define correspondence between two surfaces, one must find the Möbius transformation that best aligns two parameterizations—akin to picking a translation and rotation in rigid registration problems. We describe a simple procedure that canonically centers and rotationally aligns two spherical maps. Centering is implemented via elementary operations on triangle meshes in \mathbb{R}^3 , and minimizes area distortion. Alignment is achieved using the FFT over the group of rotations. We examine this procedure in the context of spherical conformal parameterization, orbifold maps, non-rigid symmetry detection, and dense point-to-point surface correspondence.

Categories and Subject Descriptors (according to ACM CCS): I.3.5 [Computer Graphics]: Computational Geometry and Object Modeling—Geometric algorithms, languages, and systems

1 Introduction

The *uniformization theorem* guarantees that there is a conformal map $f: S^2 \to M$ from the sphere S^2 to any genus zero surface M, *i.e.*, a smooth, nondegenerate, and globally injective map that preserves both angles and orientation. This fact is enticing for applications, since it ensures there is always a "nice" map between any two surfaces M_1, M_2 of genus zero, given by the composition

 $f_2 \circ f_1^{-1}$ of two corresponding spherical parameterizations f_1, f_2 . Not surprisingly, numerical algorithms for computing spherical conformal parameterizations have received significant attention over the past two decades [HAT*00, GY03, GGS03, FSD05, KSS06, SSP08, KSBC12, CPS13, PKC*16]. Unfortunately, however, for a given surface M the parameterization f is not unique: it is determined only up to $M\ddot{o}bius\ transformations$, i.e., conformal maps from $S^2 \to S^2$.

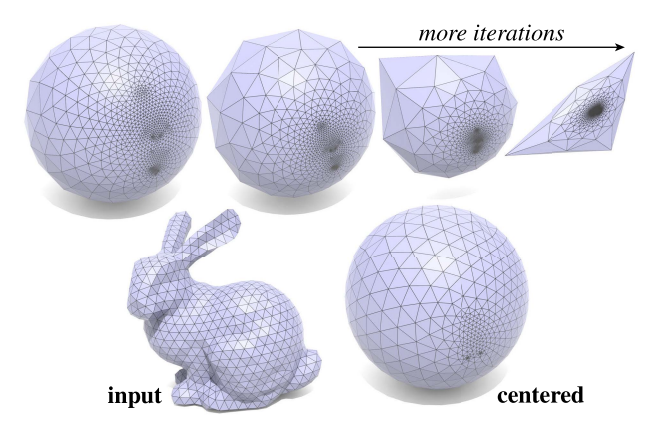


Figure 2: Top: Left unchecked, iterative algorithms for spherical conformal parameterization may apply large Möbius transformations that severely distort area. Bottom right: A basic application of our algorithm is to prevent this "drift" by picking a canonical inversion that centers area distortion.

Computing the best-aligned Möbius transformation is therefore quite important, because it allows one to define a "cross-parameterization" that is determined purely by the geometry of the two surfaces (Figure 1), without reference to auxiliary data such as landmark points. The resulting map can be used to transfer information between two similar shapes, facilitating tasks including surface matching, point-to-point correspondence, detail transfer, remeshing, and shape co-analysis. For a single surface, defining a canonical Möbius inversion plays a role in, *e.g.*, stabilizing parameterization algorithms (Figure 2), or mitigating area distortion in surface flows [CPS13].

In this paper we propose a simple, pragmatic approach that finds a centering transformation with low area distortion via a simple iterative descent algorithm, then achieves rotational alignment via a fast Fourier transform (FFT) over the group of rotations. For perfectly isometric surfaces this procedure recovers an isometry; for near-isometric surfaces we get reasonably good correspondence, though of course quality is greatly restricted by the rigidity of Möbius transformations. Therefore, one way to view our method is as a fast and reliable way to initialize more challenging (e.g., nonconvex) surface registration algorithms, whether conformal or not.

Outline After reviewing related work (§2) and relevant mathematical background (§3), we derive a simple descent strategy that is guaranteed to produce a unique centering transformation (§4). We then briefly consider a generalization to non-conformal transformations, providing a trade-off between angle and area distortion (§5). In §6 we give an explicit centering algorithm, and show how fast signal processing can be used to register the rotational component. We evaluate our approach in the context of spherical conformal parameterization, spherical orbifold mapping, non-rigid symmetry detection, and dense correspondence, highlighting some of the challenges of using conformal maps for shape registration (§7). In §8 we provide a summary and discussion of future work.

2 Related Work

The problem of finding the "best" Möbius transformation has been studied in a variety of different contexts. For some tasks (such as surface parameterization or data visualization) it is sufficient to determine a canonical inversion; for other tasks (such as surface registration) a rotation is also needed in order to align two surfaces. We consider both tasks below.

2.1 Canonical Inversion

Suppose we do not care about rotation. Which Möbius transformation is canonical? Bern and Eppstein [BE01] use quasiconvex programming to maximize the minimum radius of a collection of spheres or edge lengths, with applications to problems in data visualization and mesh generation; implementation is substantially more complicated than for the approach we present here, and optimization of nonuniform triangle areas (as arise in conformal mapping) is left as an open problem. Crane *et al.* [CPS13, Appendix E] consider Möbius transformations that minimize area distortion in the special setting of conformal surface immersions parameterized by *mean curvature half density*, with no guarantee of optimality.

More commonly, the canonical Möbius transformation is defined as the one that places the center of mass of a collection of points p_1, \ldots, p_n at the origin. Springborn [Spr05] shows that such a transformation always exists and is unique; the same basic reasoning would appear to extend to a positively-weighted sum of points or any sufficiently well-behaved mass density $\lambda: M \to \mathbb{R}_{>0}$.

Stereographic projection. Möbius transformations of the sphere have many different representations. One is to stereographically map the sphere to the plane via a point of projection $p \in S^2$, apply a rotation $\theta \in [0, 2\pi)$, offset $u \in \mathbb{R}^2$, and positive scaling $a \in \mathbb{R}_{>0}$ of the plane, then return to the sphere via inverse stereographic projection; note there are six degrees of freedom in total, corresponding to the dimension of the Möbius group. Li & Hartley [LH07, Section 4.5] directly minimize the norm of the center of mass with respect to the scaling a and offset u, which are sufficient to describe Möbius transformations up to rotation (a statement there that the minimizer can be obtained via a linear system appears to be in error [Har18]). Koehl & Hass [KH14, Section 2.3] take the same approach to find an initial guess for subsequent a nonconvex energy (note that this strategy is actually different from the one of Springborn, which we discuss below). Although the centering transformation is unique, there is no clear guarantee that gradient descent on this particular energy will always work—for instance, the norm of the center of mass is not a convex function of a and u, due to the inverse stereographic projection. Our centering procedure (Algorithm 1) provides a simple alternative that is guaranteed to find a canonical inversion.

Homogeneous coordinates. Springborn [Spr05, Lemma 2] characterizes the centering Möbius transformation as the minimizer of an energy that is geodesically convex in hyperbolic space, though is not convex with respect to any coordinates on this space. To date there is very little work on geodesic convex optimization [ZS16]; a practical alternative suggested by Springborn [Spr18] is to consider Möbius transformations of the 2-sphere $S^2 \subset \mathbb{R}^3$ represented as linear transformations in homogeneous coordinates p = (x, y, z, t). In particular, let $E \in \mathbb{R}^{4 \times 4}$ encode the *Lorentz inner*

product $p^T E p = x^2 + y^2 + z^2 - t^2$, so that homogeneous coordinates satisfying $p^{\mathsf{T}}Ep = 0$ correspond to points on the unit sphere. Möbius transformations are then represented by linear maps that preserve this inner product, and hence map the sphere to itself (the so-called Lorentz transformations). To center a collection of points $p_i = (x_i, y_i, z_i, 1)$ on the unit sphere, one first minimizes the energy $\Phi(q) = \sum_{i} \log(-q^{\mathsf{T}} E p_i / \sqrt{-q^{\mathsf{T}} E q})$ over points q = (x, y, z, 1) with (x, y, z) inside the unit ball. A Lorentz transformation is then obtained by applying the Gram-Schmidt process (relative to E) to the vectors $a_4 = q$, $a_1 = (1, 0, 0, 0)$, $a_2 = (0, 1, 0, 0)$, $a_1 = (0, 0, 1, 0)$ (in this order), which become the columns of a matrix $A = (a_1, a_2, a_3, a_4)$. The inverse matrix, $A^{-1} = EA^{\mathsf{T}}E$, gives the centering inversion. Though the Hessian of Φ is not always positive-definite, one can switch to gradient descent at indefinite points and still arrive at a canonical solution. Our strategy provides the same guarantees, but is simpler to implement and tends to converge in far fewer iterations.

Euclidean coordinates. Finally, just as every rotation of space can be expressed as an even number of reflections, every Möbius transformation of the sphere can be expressed as an even number of spherical reflections in standard Euclidean coordinates. In Section 4 we consider an elementary approach to centering based on this point of view, yielding an iterative descent scheme (Algorithm 1) that can be directly applied to triangle meshes or point sets in \mathbb{R}^3 . From a practical point of view, there appears to be no real benefit to working with stereographic projection or homogeneous coordinates: the simple Euclidean algorithm we describe is guaranteed to work, converges rapidly, and can be implemented via straightforward operations in \mathbb{R}^3 . Moreover, this perspective extends to canonical spherical parameterizations that trade off between angle and area distortion (Section 5), and in principle, provides a starting point for defining canonical mappings on any domain (not just spheres).

2.2 Conformal Registration

To establish point-to-point correspondence between surfaces, one must find the best-aligned Möbius transformation including rotation. Despite the importance of this problem, it has received relatively little attention: most earlier approaches either require landmarks (e.g., [SZS*13,LLYG14]) or perform extensive sampling of possible three-point correspondences (e.g., [LF09, LPD13]). Unlike these methods, our approach does not require landmarks or other auxiliary data, and does not need to perform extensive search. A notable exception is the method of Hass & Koehl [HK15], who optimize a more sophisticated (albeit nonconvex) measure of metric distortion; the resulting notion of canonical metric appears to be quite valuable for problems in shape matching and analysis [KH14, KH15]. In this context, our centering strategy can be viewed as a replacement for their initialization procedure. Finally, Li & Hartley [LH07] consider a rotation invariant shape descriptor using spherical harmonics relative to a canonical Möbius inversion. This descriptor cannot however be used to determine point-to-point correspondence.

A simple idea for performing rotational alignment is to apply principal component analysis to conformal scale factors, but this approach merely aligns quadratic terms in the Fourier expansion—ignoring the large "spikes" of area distortion typically seen in a conformal parameterization. A more sophisticated idea is to apply

Fourier-type methods directly to the Möbius group—here one encounters two challenges. First, the group of Möbius transformations is not compact, making it impossible to use existing generalizations of the Fast Fourier Transform (FFT) [MR95, Roc97]. Second, the Möbius group is six-dimensional, so even if a signal-processing approach were possible, the storage and run-time requirements would be prohibitively expensive. From this point of view, finding a canonical inversion can also be viewed as a way of reducing the dimensionality of the problem, allowing us to facilitate a (lower-dimensional) signal processing approach to achieve alignment (Section 6).

3 Review

We first review some basic facts and notation that are needed to derive our basic centering algorithm.

3.1 Notation

Throughout we will use $|\cdot|$ and $\langle\cdot,\cdot\rangle$ to denote the usual Euclidean norm and inner product on vectors in \mathbb{R}^3 . For any time-varying quantity $\phi(t)$ we will use a single dot to denote the derivative at time zero, *i.e.*,

$$\dot{\phi} := \left. \frac{d}{dt} \right|_{t=0} \phi.$$

3.2 Möbius Transformations of the Sphere

Consider the open unit ball in \mathbb{R}^3 given by the set of points

$$B^3 := \left\{ x \in \mathbb{R}^3 : |x| < 1 \right\}.$$

and let S^2 be the boundary of B^3 , *i.e.*, the unit sphere. For any *center* $c \in B^3$, we can compose a spherical reflection $x \mapsto (x+c)/|x+c|^2$ with translation and scaling to obtain a map

$$\eta_c(x) := (1 - |c|^2) \frac{x + c}{|x + c|^2} + c$$

that takes S^2 to S^2 (as illustrated in Figure 3). We will refer to such maps as *inversions*. All conformal maps from the sphere to itself (including rotations) can be expressed as an even number of inversions—though for the purpose of centering (where we do not care about rotation, and where orientation is superficial) we can consider just a single inversion.

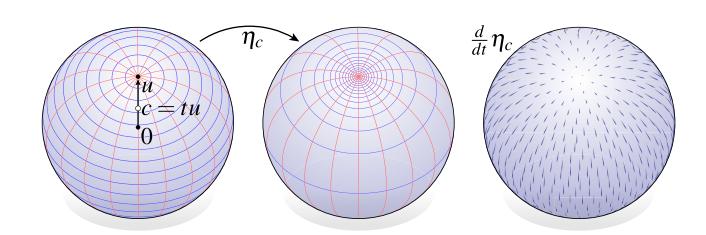


Figure 3: Left: An inversion η_c will push the sphere toward the inversion center c. Right: If c(t) = tu is a time-varying family of centers (for some fixed vector u), then the motion $\frac{d}{dt}\eta_c$ looks like a flow toward c along the gradient of the linear function $\langle u, x \rangle$.

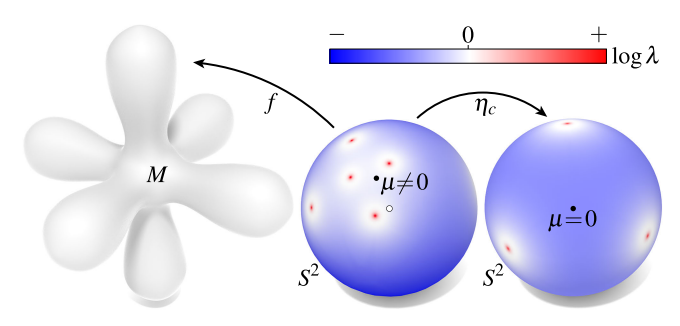


Figure 4: A spherical conformal parameterization $f: S^2 \to M$ distorts area by a factor λ . Viewing λ as a mass density on the sphere, we seek an inversion η_c that puts the center of mass at the origin.

4 Canonical Centering

Let $f: S^2 \to M$ be a spherical conformal parameterization of a genus zero surface $M \subset \mathbb{R}^3$. The area element dA on M is then related to the standard area element dA_{S^2} on the sphere by

$$dA = \lambda dA_{S^2}$$
,

where the function $\lambda: S^2 \to \mathbb{R}_{>0}$ is called the *conformal scale factor*. We will use $\mu_0 \in \mathbb{R}^3$ to denote the corresponding *center of mass*

$$\mu_0 := \int_{S^2} \lambda(x) x \, dA_{S^2} = \int_{S^2} x \, dA,\tag{1}$$

i.e., the position x on the sphere, weighted by the conformal factor λ . Suppose we apply an inversion η_c to the sphere, yielding a new parameterization $f \circ \eta_c^{-1}$ with conformal factors λ_c . Then the new center of mass is

$$\mu(c) := \int_{S^2} \lambda_c(x) x \, dA_{S^2} = \int_{S^2} \eta_c(x) \, dA, \tag{2}$$

since when the integral on the left is pulled back under η_c , the conformal scaling due to the η_c^{-1} component of $f \circ \eta_c^{-1}$ cancels with the change in area due to the pullback. We seek an inversion that moves the center of mass to the origin (i.e., $\mu(c)=0$), which can be acheived by minimizing the energy

$$E := \frac{1}{2} |\mu(c)|^2$$

with respect to the inversion center c. (Note that we do not need to consider rotations, which have no effect on the norm.) The corresponding gradient is given by

$$\nabla_c E = J_{\mu}^{\mathsf{T}} \mu, \tag{3}$$

where J_{μ} denotes the Jacobian of μ with respect to c (and ^T denotes the transpose). To compute this Jacobian, consider a time-varying inversion center c(t) := tu for some fixed vector $u \in \mathbb{R}^3$. The time derivative of η_c at t = 0 is then

$$\frac{1}{2}\dot{\eta}_{c(t)}(x) = u - \langle u, x \rangle x.$$

In other words, moving the center of inversion toward u causes each point x to slide tangentially on the sphere, along the direction closest to u. As a result, the sphere will gradually contract near the head of u, and expand near its tail (consider Figure 3, right). Applying our

expression for $\dot{\eta}$ to Equation 2, we then get

$$\dot{\mu} = 2 \int_{S^2} u - \langle u, x \rangle x \, dA.$$

Noting that $J_{\mu}u = \dot{\mu}$ for all u, the Jacobian at c = 0 is therefore

$$J_{\mu}|_{c=0} = 2 \int_{\mathbb{S}^2} \operatorname{id} - x \otimes x \, dA, \tag{4}$$

where id denotes the identity, and \otimes is the outer-product.

4.1 Existence and Uniqueness

Following the gradient $\nabla_c E$ will always yield a unique center $c \in B^3$ that places the center of mass μ at the origin. To see why, first note that the Jacobian J_{μ} has full rank, since it is a positive linear combination of linearly independent rank-2 operators id $-x \otimes x$. Hence, the energy gradient $\nabla_c E = J_{\mu}^T \mu$ will be zero if and only if $\mu_0 = 0$, *i.e.*, if the center of mass is already at the origin. Moreover, as the center approaches the boundary of the ball, the energy tends toward its *maximum* value, *i.e.*, $\lim_{|c| \to 1} E = c \int_{S^2} dA$. Hence, there must be a minimum at some point on the interior of B^3 . To see that the centering inversion is unique, recall that an inversion moves each point toward the centering direction c (except for the poles $\pm c$). Hence,

$$\langle c, \eta_c(x) \rangle \geq \langle c, x \rangle.$$

Suppose the center of mass is already at the origin, *i.e.*, $\mu_0 = 0$, and let $\mu(c)$ be the center obtained by applying an inversion with any center $c \in B^3$. Then

$$\langle c, \mu(c) \rangle = \int_{\mathcal{S}^2} \langle c, \eta_c \rangle \ dA > \int_{\mathcal{S}^2} \langle c, x \rangle \ dA = \langle c, \mu_0 \rangle = 0.$$

(Note that the inequality is strict since λ is a smooth function; hence, not all mass can be concentrated at the poles.) Hence, there can be no inversion that leaves the center of mass at the origin.

5 Generalized Centering

In Section 4 we studied the centering problem via explicit geometric calculations in \mathbb{R}^3 . In this section we consider an alternative, functional perspective that naturally generalizes beyond conformal transformations of the sphere. To make a link between the two points of view, suppose that $x=(x_1,x_2,x_3)$ are coordinates on \mathbb{R}^3 . Then we can think of μ as the projection of the conformal factor λ onto the space of linear functions spanned by the corresponding coordinate functions $e_i: S^2 \to \mathbb{R}; x \mapsto x_i$. In other words, we can identify μ with the function $\frac{3}{4\pi} \sum_{i=1}^3 (\int_{S^2} \lambda \ e_i \ dA_{S^2}) e_i$. Additionally, infinitesimal inversions look like gradients of linear functions, *i.e.*, for c(t) = tu, we have

$$\frac{1}{2}\dot{\boldsymbol{\eta}}_{c(t)}(x) = u - \langle u, x \rangle x = \nabla \langle x, u \rangle,$$

as depicted in 3, right. Hence, the center of mass μ is zero if and only if the conformal factors vanish when projected onto the space of linear functions; if μ is nonzero, then we can always reduce its norm by "flowing" along the gradient of some linear function. Rather than thinking about conformal factors, we could also just say: the parameterization is centered if the coordinate functions on S^2 vanish when integrated with respect to the area of the target surface. As we will see in Section 5.2, the notion of a centered parameterization can

therefore be generalized by replacing the linear functions with any collection of smooth functions \mathcal{F} , and the area element dA with a volume form ω on any manifold. Likewise, our centering motions will no longer be infinitesimal Möbius transformations, but rather flows along gradients of functions in \mathcal{F} . The key observation is that, as with the sphere, a parameterization that is not centered can always be improved by such motions, *i.e.*, the norm of the center μ has local minima only when $\mu = 0$.

5.1 Preliminaries

We briefly review some basic concepts needed for our generalization; more detailed discussion can be found in a standard text on differentiable manifolds, such as Abraham *et al.* [AMR93]. Let M be a compact connected orientable n-manifold without boundary, and let dV be the volume form on M—in the context of Section 4, for instance, $M = S^2$ and $dV = dA_{S^2}$. We will use $\|\cdot\|$ and $\langle\langle\cdot,\cdot\rangle\rangle$ to denote the L^2 norm and inner product (resp.) with respect to dV.

A smooth vector field X on M defines a *flow map* $F_{X,t}: M \to M$ obtained by following integral curves of X for time t; this map is always well-defined and invertible up to some sufficiently small time T > 0. We will use $(F_{X,t})_*\omega$ to denote the pushforward of an n-form ω under such a flow. The *Lie derivative*

$$\mathcal{L}_X \omega := \left. \frac{d}{dt} \right|_{t=0} (F_{-X,t})_* \omega \tag{5}$$

then describes the infinitesimal change in ω as we advect it along -X. For any scalar function ϕ , the Lie derivative satisfies a product rule $\mathcal{L}_X(\phi\omega) = \phi \mathcal{L}_X\omega + (\mathcal{L}_X\phi)\omega$, and for an n-form on a manifold without boundary we have $\int_M \mathcal{L}_X(\phi\omega) = 0$ (by Cartan's formula and Stokes' theorem). Hence,

$$\int_{M} \phi \mathcal{L}_{X} \omega = -\int_{M} (\mathcal{L}_{X} \phi) \omega, \tag{6}$$

i.e., under a flow along X, integration of a function ϕ simply changes by (minus) the directional derivative of f along X. For scalar functions, the Lie derivative is just the directional derivative, *i.e.*, $\mathcal{L}_X \phi = \langle X, \nabla \phi \rangle$, where $\nabla \phi$ is the gradient of ϕ .

5.2 Generalized Centering

Consider a k-dimensional space of functions $\mathcal{F} \subset W^{1,2}(M)$, none of which are constant. We define the *center of mass* of a volume form ω relative to \mathcal{F} as the unique function $\mu_0(\omega) \in \mathcal{F}$ satisfying

$$\langle\langle\psi,\mu_0(\omega)\rangle\rangle = \int_M \psi\omega$$
 (7)

for all $\psi \in \mathcal{F}$. Equivalently, if \mathcal{F} has an orthonormal basis e_1,\ldots,e_k , then $\mu_0(\omega) = \sum_{i=1}^k \left(\int_M e_k \omega \right) e_k$, *i.e.*, $\mu_0(\omega)$ is effectively the "projection" of ω onto \mathcal{F} . For any function $\phi \in \mathcal{F}$, we then define

$$\mu(\phi) := \mu_0((F_{\nabla \phi,1})_*\omega)$$

as the center of mass obtained by flowing the volume form ω along the gradient of ϕ . We say that ϕ *centers* ω (with respect to \mathcal{F}) when $\mu(\phi)=0$, and can measure how far we are from being centered via the energy

$$E := \frac{1}{2} \|\mu\|^2$$
.

We then get a result that generalizes the one we had for inversions:

Theorem: If $\mu(\phi) \neq 0$, then there is a function $\psi \in \mathcal{F}$ such that flowing ω along the gradient vector field $X = \nabla \psi$ reduces the quantity $\|\mu\|^2$, *i.e.*, we can always bring $\mu(\phi)$ closer to the origin.

Proof: We proceed essentially as in Section 4: the gradient of the energy E can be expressed as $\nabla_{\phi}E = J_{\mu}^{\mathsf{T}}\mu$, where $J_{\mu}: \mathcal{F} \to \mathcal{F}$ denotes the Jacobian of μ with respect to ϕ . To evaluate $J_{\mu}\psi$ at $\phi=0$, consider a time-varying function $\varphi(t)=t\psi$ for any fixed function $\psi\in\mathcal{F}$. Then

$$J_{\mu}\psi\big|_{\phi=0} = \left. \frac{d}{dt} \right|_{t=0} \mu(\varphi(t)) = \left. \frac{d}{dt} \right|_{t=0} \mu_0((F_{\nabla \psi,t})_* \omega).$$

Taking the L^2 inner product with ψ and applying Equation 7 gives

$$\langle\langle \psi, J_{\mu} \psi \rangle\rangle\big|_{\phi=0} = \int_{M} \psi \left. \frac{d}{dt} \right|_{t=0} (F_{\nabla \psi, t})_* \omega,$$

and applying Equations 5 and 6 then yields

$$\langle\langle\psi,J_{\mu}\psi\rangle\rangle\big|_{\phi=0} = \int_{M} \psi \mathcal{L}_{-\nabla\psi}\omega = \int_{M} (\mathcal{L}_{\nabla\psi}\psi)\omega = \int_{M} \langle\nabla\psi,\nabla\psi\rangle\omega.$$

Since \mathcal{F} contains no constant functions, $\nabla \psi$ must be nonzero; moreover, ω is a volume form and hence positive everywhere. As in the case of inversions, then, the Jacobian J_{μ} is strictly positive definite, and hence the energy gradient ∇E will vanish at $\phi = 0$ if and only if $\mu_0(\omega)$ is zero, *i.e.*, if ω is centered.

Uniqueness of the centering motion is less clear—the argument used for Möbius transformations of the sphere was purely geometric, and hence does not generalize to the functional setting. Note that in practice, J_{μ} is just a real $k \times k$ matrix which can be used to implement a descent algorithm that looks identical to Algorithm 1; here the function ϕ plays the role of the center c, and inversion is replaced by advection along $\nabla \phi$.

Example: Higher-Order Harmonics

A trivial example of centering in this framework would be to let \mathcal{F} be the linear functions on $M = \mathbb{R}^n$; in this case our procedure flows mass along the corresponding constant vector fields, which is the same as just translating the center of mass to the origin. As a more interesting example we return to the case of the sphere,

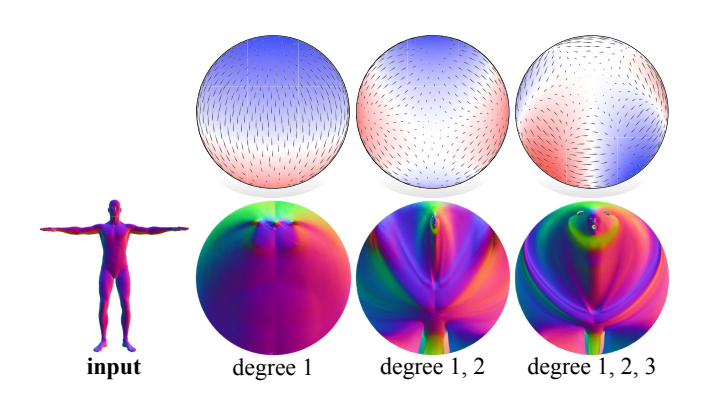


Figure 5: By considering centering motions beyond just Möbius transformations, we can trade off between area and angle distortion. Here we use gradients of spherical harmonics of increasing degree.

and seek a parameterization that is centered with respect to some collection of "low-frequency" functions—in particular, we let $\mathcal F$ consist of low-order spherical harmonics, as shown in Figure 5. For degree-one harmonics (just linear functions) we get only infinitesimal inversions; for progressively higher order harmonics we get additional, non-conformal motions that allow better distribution of area, at the cost of angle distortion. This picture also makes it clear that our Möbius centering procedure eliminates any "low-frequency" area distortion, since the linear component of the conformal scale factors λ vanishes. Here and in similar experiments we find that our procedure always yields a centered parameterization ($\mu(\omega)=0$).

Non-Gradient Flows

In addition to transformations characterized by flows along gradients of functions, one would also like to consider transformations along divergence-free vector fields. Unfortunately, our centering approach does not extend to these cases and we believe that centering with respect to divergence-free transformations is much harder. In the case of the sphere, for example, inversions are characterized by the gradients of linear functions. Applying a pointwise 90-degree rotation, we obtain the complimentary space of divergence-free vector fields. These characterize (infinitesimal) rotations, completing the group of Möbius transformations. As we cannot center with respect to them, the next section describes and efficient approach for aligning over the space of rotations.

6 Möbius Registration

We now consider the task of finding correspondence between two genus zero surfaces, which we perform in three steps: first compute a conformal parameterization of each surface over the sphere, using any method (see references in Section 1), find canonical centering inversions (Section 6.1), and finally compute the rotation that best aligns the two centered parameterizations (Section 6.2). Though our method can in principle be applied to any surface representation, we give an explicit algorithm for triangle meshes. We will assume that each input mesh is encoded by a collection of triangles T with areas $A : \to \mathbb{R}_{>0}$ from the original surface M, and will assume that the vertices $V \subset S^2$ have already been mapped to the unit sphere S^2 . (To instead apply our algorithm to a set of points $P \subset S^2$, one can simply replace the triangle centers with P and the triangle areas with $A \equiv 1$ in Algorithm 1.) A complete implementation of this procedure, including spherical parameterization, can be found at https://github.com/mkazhdan/MoebiusRegistration.

6.1 Centering Algorithm

The analysis in Section 4 suggests a simple algorithm for centering a given parameterization: simply perform gradient descent on the energy E with respect to the inversion center c, starting at any point in B^3 . Since the gradient vanishes only at the global minimum (and the energy goes to $\frac{1}{2} \left(\int_{S^2} \omega \right)^2$ as c approaches the boundary of B^3), we will always obtain a canonical centering, up to rotation. Since we have an explicit expression for the Jacobian J_{μ} of the center with respect to c, this algorithm can easily be accelerated using Gauss-Newton iterations rather than simple gradient iterations, as shown in Algorithm 1. Here, $C(\tau)$ denotes the center of mass of a triangle

Algorithm 1 MÖBIUSCENTER (T, V, A, ε)

Input: A mesh with triangles T, areas $A: T \to \mathbb{R}_{>0}$, a conformal parameterization specified by vertex coordinates $V \subset S^2$, and a stopping tolerance $\varepsilon > 0$. $(C(\tau)$ denotes the center of τ , normalized to have unit length.)

Output: Centered vertex coordinates $V \subset S^2$.

```
1: while true
          \mu \leftarrow \sum_{\tau \in T} C(\tau) A(\tau)
                                                              2:
          if |\mu| \le \varepsilon then break
3:
          J_{\mu} \leftarrow 2\sum_{\tau \in T} A(\tau)(I - C(\tau)C(\tau)^{\mathsf{T}})
4:

    build Jacobian

         c \leftarrow J_{\mu}^{-1} \mu
for \ v \in V
v \leftarrow (1 - |c|^2) \frac{v + c}{|v + c|^2} + c
                                                            > compute inversion center
5:
6:
7:

    □ apply inversion

8: return V
```

 τ ; for simplicity we use the average of its vertices. We do not need to explicitly compute the conformal scale factors λ , since they are already accounted for by the area weights A. The simple form of the Gauss-Newton update arises from the fact that J_{μ} is symmetric, and hence $-(J_{\mu}^{\mathsf{T}}J_{\mu})^{-1}J_{\mu}^{\mathsf{T}} = -J_{\mu}^{-1}$. Here we use a unit time step, though for larger or more challenging models it may be helpful to take a smaller step (i.e., replace c with αc for some constant $\alpha \in (0,1)$) or perform an explicit line search (setting the energy of centers c outside the unit ball to infinity). Note that this algorithm assumes that vertices v are on the *unit* sphere, i.e., $|v|^2 = 1$; it will not work properly for spheres of other radii.

Generalized centering. To center with respect to a general collection of functions \mathcal{F} with orthonormal basis e_1,\ldots,e_k , we make two modifications to Algorithm 1. First, $C(\tau)$ returns a vector containing the value of each basis function at the triangle center. Second, the transformation in Line 7 is replaced by numerical advection of the spherical triangulation along the gradient of c, which is now viewed as a function on M. That is, we move each vertex along the surface M with velocity determined by the gradient. Here one must be careful to take sufficiently small time steps, in order to avoid triangle flips.

6.2 Rotational Alignment

We next seek the rotation that best aligns the two parameterizations. To do so, we first sample the conformal factors of each mesh onto a regular spherical grid (Figure 6, top right). We then find the rotation that maximizes the correlation between conformal factors, via a fast spectral transform.

Sampling conformal factors. Given a centered mesh (V,T) with original areas $A:V\to\mathbb{R}_{>0}$, we compute the total area contained in each cell of a regular spherical grid, divided by the area of the spherical cell—these values represent the average conformal factor over the cell (Figure 6, bottom right). Note that simply *sampling* the area ratio at the cell center can yield significant aliasing, since a conformal parameterization may map a large region of the mesh to a very small region on the sphere. We likewise apply a low-pass filter to further reduce potential aliasing (Figure 6, bottom left).

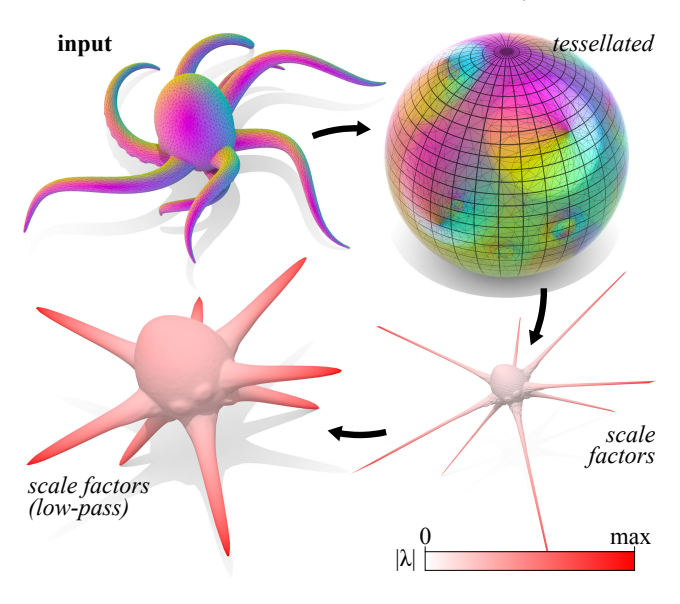


Figure 6: Prior to rotational alignment, the input mesh (top left) is parameterized, centered, and tessellated by an equirectangular grid (top right). Sampled conformal factors (bottom right) are then low-pass filtered (bottom left) to mitigate aliasing. (Scale factors are visualized by scaling points on the unit sphere according to $|\lambda|$.)

Aligning conformal factors. To obtain our final registration, we compute the rotation that maximizes the correlation between the scale factors sampled from the two meshes. This rotation is obtained in three steps: (1) We compute the forward fast spherical harmonic transform [HRKM03] to get an expression of each spherical function in terms of the spherical harmonics. (2) We cross-multiply the spherical harmonic coefficients within each frequency band to obtain the coefficients of the correlation in terms of the rotational harmonics. (3) We apply the fast inverse Wigner-D transform [KR08] to obtain a sampling of the correlation on a regular 3D grid of Euler angles. Since the input functions are band-limited, the correlation function is also band-limited; to robustly detect maxima we use a regular grid whose resolution is twice the band-width. To get an orientation-reversing registration (e.g., for reflective symmetry detection), we can simply apply a reflection to one of the two sampled functions. Note that if either shape has rotational symmetries we will of course obtain only one possible registration; this ambiguity is a fundamental feature of the registration problem (and has nothing to do with our particular algorithm).

7 Evaluation

To evaluate our approach we consider four applications: stabilizing a spherical conformal parameterization algorithm, computing spherical orbifold parameterizations, detecting non-rigid intrinsic symmetry, and finding dense point-to-point correspondence. The first two examples demonstrate the utility of our approach; the latter two illustrate some of the challenges faced when using conformal parameterization for surface registration. We also provide some basic information about performance.

7.1 Stabilizing Conformal Parameterization

In principle, one might expect algorithms for spherical conformal parameterization to be oblivious to Möbius transformations, but in reality discretization error causes certain Möbius transformations to be preferred. For instance, one way to obtain a conformal map is to minimize Dirichlet energy, which for the sphere is naturally discretized as $\frac{1}{4}\sum_{e}w_{e}\theta_{e}^{2}$, where θ_{e} is the angle between the endpoints of an edge e (i.e., an arc on the sphere S^{2}), and w_{e} is the corresponding cotangent weight (from the input domain M). A trivial way to minimize this energy is to move all vertices to a common point, and this is exactly the kind of behavior observed in many iterative algorithms: the parameterization "drifts" toward a Möbius transformation that concentrates all vertices at a point. We can prevent this behavior by simply applying our centering algorithm (Algorithm 1), as demonstrated in Figure 2 for a conformal map computed via conformalized mean curvature flow (CMCF) [KSBC12].

7.2 Spherical Orbifold Parameterization

A spherical orbifold is a quotient of the sphere S^2 by a finite group of rotations—intuitively, a tiling of the sphere. Conformal parameterization over such domains has recently been explored as a way to reduce area distortion for genus zero surfaces [AKL17]. We consider a different algorithmic approach: first, we create a multiple covering \widetilde{M} of the input geometry M, then we compute a conformal parameterization of this covering over the sphere. By centering this

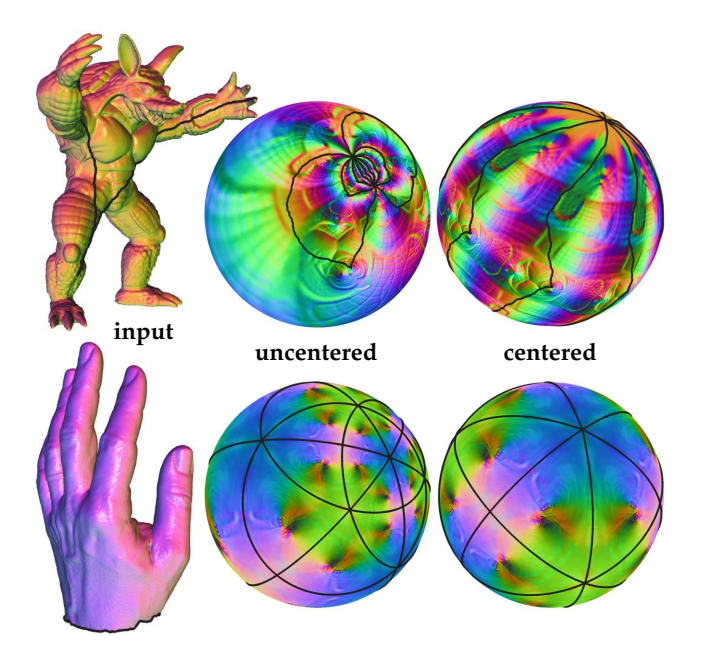


Figure 7: Spherical orbifold maps with cyclic symmetry (top) and tetrahedral symmetry (bottom). Though an arbitrary spherical conformal parameterization of a covering space might not be rotationally symmetric (center), our centering procedure ensures that it exhibits the desired orbifold symmetry (right). Black lines indicate cuts made on the input mesh (left).

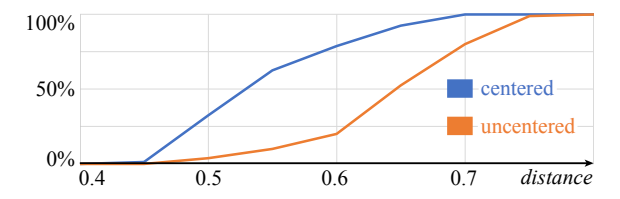


Figure 8: Cumulative distribution of reflective symmetry distances for the TOSCA high-resolution models.

parameterization, we ensure that it exhibits the same rotational symmetry as the target orbifold. To construct the covering surface we cut the surface M along an open curve; we then glue together multiple copies of the cut surface M^* . For instance, to get a covering with a cyclic symmetry group C_n we make n copies M_1^*, \ldots, M_n^* (each with the same triangle areas as M), and glue the "right" side of the cut on M_i^* to the "left" side of the cut on M_{i+1}^* (modulo n). We then conformally parameterize the covering surface M via CMCF, which entails little more than iteratively solving a discrete Poisson problem involving the cotangent Laplacian. Though the initial map may not exhibit rotational symmetry (Figure 7, middle), centering this map yields the desired result (Figure 7, bottom). Compared with the method of Aigerman et al. [AKL17] this construction is conceptually much simpler: we do not need to carefully determine and implement boundary conditions; we simply need to construct a covering space with the desired topology, and build a standard Laplace matrix on a domain without boundary. On the other hand, our system is *n* times larger, and we guarantee nothing about injectivity.

7.3 Non-rigid Bilateral Symmetry Detection

Many common shapes (such as the human body) exhibit strong bilateral symmetry. Even if such a shape has been deformed nonrigidly (e.g., by bending an arm), this symmetry can be detected by seeking an orientation-reversing map $M \rightarrow M$ that is close to an isometry. In our setting, this means looking for the anti-conformal map $\eta: S^2 \to S^2$ that best preserves the conformal scale factors λ of a spherical parameterization. A nice property of our centering procedure is that it will yield a parameterization with reflective symmetry, if one exists: since the gradient of a symmetric configuration always lies in the plane of symmetry (and inversion in such a point preserves symmetry), starting at a symmetric configuration will yield a symmetric minimizer. But since the minimizer of our energy is unique, any parameterization that admits symmetric scale factors will have a symmetric minimizer. To detect bilateral symmetry, we can therefore center our parameterization, then compute the best orientation-reversing registration of the surface with itself (as described at the end of Section 6.2).

To gauge the effectiveness of this procedure we applied it to the TOSCA high-resolution dataset [BBK08], which consists of 80 non-rigidly deformed models across 9 different categories. (For models with several connected components we used the component with largest area; we also performed hole-filling when necessary.) For each model, we computed a conformal parameterization using CMCF, and sampled scale factors onto a 256×256 equirectangular grid. Figure 8 shows the cumulative distribution of bilateral symme-

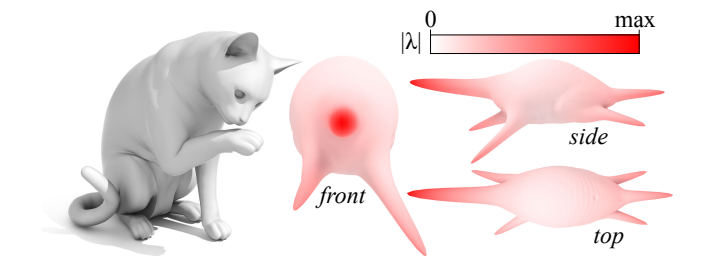


Figure 9: To measure bilateral symmetry of a given mesh (left), we compute a centered conformal parameterization, then look for an orientation-reversing orthogonal transformation that best preserves the conformal scale factors λ (right), here visualized as a normal offset from the unit sphere.

try distances for these models, with and without centering. Distance values are normalized to the range [0,1], with smaller distances corresponding to parameterizations with greater reflective symmetry. As expected, we find that centering significantly improves symmetry detection (since arbitrary Möbius transformations do not preserve reflective symmetry). However, the distances are still perhaps larger than one might expect, given that all models have reflective symmetry in their unposed state. Consider for instance the cat model pictured in Figure 9 (left), which exhibits a relatively large symmetry distance. As seen in Figure 9 (right), the conformal scale factors exhibit relatively poor reflective symmetry, e.g., the front paws are not aligned, and are stretched by different amounts. In other words: the deformation is not a perfect isometry. To get a better measure of symmetry, one might replace the simple L^2 distance with a more sophisticated distance measure (e.g., based on optimal transport [LPD13]); exploring our generalized centering procedure in this context might also prove useful. It is also worth noting that perturbations of the metric yield smooth changes in the parameterization only when they are real analytic [FK17], which may cause instability for certain kinds of deformations.

7.4 Dense Correspondence

Möbius registration also provides dense point-to-point correspondence between source and target models $(T_1, V_1), (T_2, V_2)$. After applying the procedure from Section 6, we map each source vertex $v \in V_1$ to the target surface by locating the spherical triangle $\tau \in T_2$ containing v; the barycentric coordinates of v in τ give a map back to the original target surface. Figure 10 shows an example from the TOSCA dataset; the map between surfaces is visualized by placing each vertex of the source mesh at the corresponding location on the target mesh. Here we get reasonable correspondence on the torso, but imprecise alignment of appendages (e.g., the legs on the source are mapped just below the legs on the target). Since these features are represented by extremely small regions on the sphere, even small amounts of non-isometric deformation (visualized in Figure 10, bottom right) can result in large alignment errors. As with symmetry detection, one might therefore use this procedure to initialize a more sophisticated (albeit more expensive) correspondence algorithm.

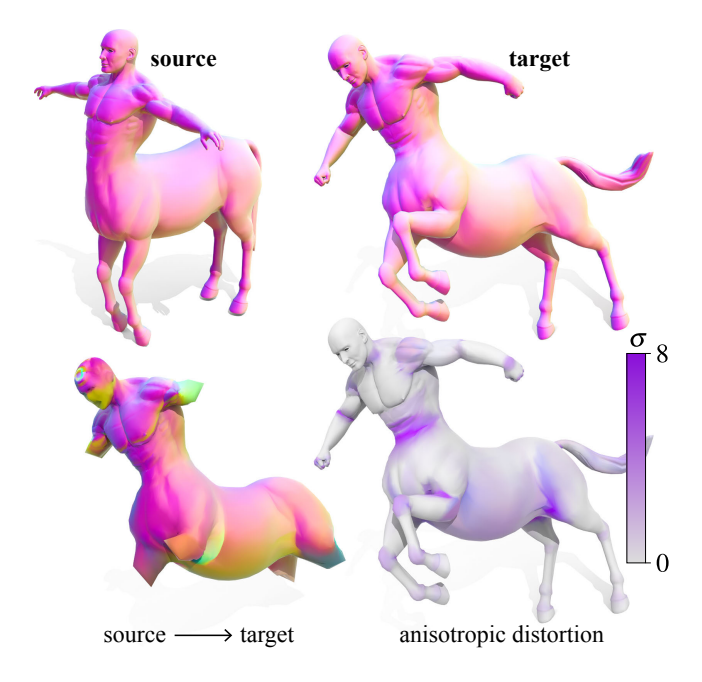


Figure 10: Dense correspondence between source and target models (top) is visualized by placing each vertex of the source mesh at the corresponding location on the target mesh (bottom left). Nonisometric deformation (bottom right) can cause substantial misalignment of features that are mapped to small regions on the sphere (anisotropy σ is the ratio of larger to smaller singular value).

model	vertices	center	tessellate	correlate
octopus	10K	0.01	0.2 / 0.4 / 1.3	0.3 / 2.2 / 27
centaur	16K	0.02	0.2 / 0.4 / 1.2	0.2 / 2.1 / 27
cat	28K	0.02	0.3 / 0.6 / 1.5	0.3 / 2.2 / 30
Michael	53K	0.06	0.3 / 0.6 / 1.4	0.3 / 2.2 / 28
hand	66K	0.09	0.7 / 1.1 / 2.7	0.3 / 2.2 / 28
bunny	104K	0.09	0.9 / 1.6 / 3.5	0.3 / 2.2 / 28
armadillo	173K	0.17	1.0 / 1.6 / 3.3	0.3 / 2.2 / 27

Table 1: Timings for the different stages of processing. For tessellation and correlation we use equirectangular grids of resolution N = 128, 256, and 512. All times are in seconds.

7.5 Performance

Table 1 gives timings for Möbius centering, spherical tessellation, and correlation, for several models and at several different grid resolutions. Timings were measured on a Windows PC with an Intel Core i7-6600 processor and 16 GB of RAM. The centering procedure appears to have linear complexity, typically achieving a center norm of about 10^{-10} in three or four iterations. Tessellation is less efficient, but still linear in the number of vertices (absolute cost depends on the number of grid cells containing each triangle). The cost of computing the final rotational correlation is independent of mesh complexity; for an $N \times N$ grid, the inverse Fourier transform over the rotation group has a cost in $O(N^4)$.

8 Conclusion

The allure of uniformization is that it provides a near-canonical map between surfaces of equivalent topology, but as we have seen, working purely in the conformal setting can be quite restrictive when it comes to applications. Other, more flexible notions of canonical mappings have the potential to be quite powerful in geometry processing—though many questions remain to be explored. Ideally, one would like to find maps that are not only canonical, but also exhibit low metric distortion (i.e., small distortion of both angles and areas). Replacing the geometric picture of Möbius transformations with the more functional picture introduced in Section 5 yields an enticing framework for this problem, with many questions that remain to be explored. For instance, we know very little about the conditions under which the generalized center exists and is unique; we also have no strategy for centering with respect to nonintegrable motions (i.e., vector fields that do not arise from a scalar potential). It is also natural to consider more informative notions of distance beyond L^2 (e.g., the Wasserstein distance), or centering with respect to other conformally invariant 2-forms (e.g., the square-norm of the gradient of the heat-kernel-signature). Finally, there is the question of how different choices of centering motions (i.e., different choices of the space \mathcal{F}) impact geometric properties of the centered parameterization. For instance, one can always use the Laplacian eigenfunctions to get a space of low-frequency deformations, but it is not clear that these motions are ideal for, e.g., minimizing metric distortion. Overall, we are hopeful that the functional, flow-based point of view will spark new ideas about how to define and construct canonical maps between surfaces, just as it has provided a valuable perspective on canonical Möbius transformations of the sphere.

Acknowledgements

Thanks to Boris Springborn and Richard Hartley for discussions about their algorithms, and Northside Social for providing collaborative work space. Thanks to Patrice Koehl for feedback on practical implementation of Gauss-Newton. This work was sponsored in part by NSF Awards 1717320 and 1422325, and gifts from Autodesk Research and Adobe Research.

References

[AKL17] AIGERMAN N., KOVALSKY S., LIPMAN Y.: Spherical orbifold Tutte embeddings. ACM Trans. Graph. 36 (2017), 90:1–90:13. 7, 8

[AMR93] ABRAHAM R., MARSDEN J., RATIU T.: Manifolds, Tensor Analysis, and Applications. Applied Mathematical Sciences. Springer New York, 1993. 5

[BBK08] BRONSTEIN A., BRONSTEIN M., KIMMEL R.: Numerical Geometry of Non-Rigid Shapes. Springer Publishing Company, Incorporated, 2008. 8

[BE01] BERN M. W., EPPSTEIN D.: Optimal Möbius transformations for information visualization and meshing. CoRR cs. CG/0101006 (2001).

[CPS13] CRANE K., PINKALL U., SCHRÖDER P.: Robust fairing via conformal curvature flow. ACM Trans. Graph. 32, 4 (July 2013), 61:1– 61:10. 1, 2

[FK17] FELDER G., KAZHDAN D.: Divergent integrals, residues of Dolbeault forms, and asymptotic Riemann mappings. *International Mathematics Research Notices* 2017 (2017), 5897–5918.

[FSD05] FRIEDEL I., SCHRÖDER P., DESBRUN M.: Unconstrained spherical parameterization. In ACM SIGGRAPH 2005 Sketches (2005). 1

- [GGS03] GOTSMAN C., GU X., SHEFFER A.: Fundamentals of spherical parameterization for 3D meshes. ACM Trans. Graph. 22, 3 (2003), 358– 363. 1
- [GY03] GU X., YAU S.-T.: Global conformal surface parameterization. In Proceedings of the 2003 Eurographics/ACM SIGGRAPH Symposium on Geometry Processing (2003), pp. 127–137. 1
- [Har18] HARTLEY R.:. personal communication, June 2018. 2
- [HAT*00] HAKER S., ANGENENT S., TANNENBAUM A., KIKINIS R., SAPIRO G., HALLE M.: Conformal surface parameterization for texture mapping. *IEEE Transactions on Visualization and Computer Graphics* 6, 2 (2000), 181–189. 1
- [HK15] HASS J., KOEHL P.: A Metric for genus-zero surfaces. arXiv e-prints (July 2015). 3
- [HRKM03] HEALY D., ROCKMORE D., KOSTELEC P., MOORE S.: FFTs for the 2-sphere-improvements and variations. *Journal of Fourier Analysis* and Applications 9, 4 (2003), 341–385. 7
- [KH14] KOEHL P., HASS J.: Automatic alignment of genus-zero surfaces. IEEE Transactions on Pattern Analysis and Machine Intelligence 36, 3 (March 2014), 466–478. 2, 3
- [KH15] KOEHL P., HASS J.: Landmark-free geometric methods in biological shape analysis. *Journal of The Royal Society Interface 12*, 113 (2015). 3
- [KR08] KOSTELEC P. J., ROCKMORE D. N.: FFTs on the rotation group. Journal of Fourier Analysis and Applications 4, 2 (2008), 145–179.
- [KSBC12] KAZHDAN M., SOLOMON J., BEN-CHEN M.: Can mean-curvature flow be modified to be non-singular? *Comput. Graph. Forum 31*, 5 (2012), 1745–1754. 1, 7
- [KSS06] KHAREVYCH L., SPRINGBORN B., SCHRÖDER P.: Discrete conformal mappings via circle patterns. ACM Trans. Graph. 25, 2 (2006), 412–438.
- [LF09] LIPMAN Y., FUNKHOUSER T.: Möbius voting for surface correspondence. *ACM Trans. Graph.* 28 (2009), 72:1–72:12. 3
- [LH07] LI H., HARTLEY R. I.: Conformal spherical representation of 3D genus-zero meshes. *Pattern Recognition* 40 (2007), 2742–2753. 2, 3
- [LLYG14] Lui L. M., Lam K. C., Yau S.-T., Gu X.: Teichmuller mapping (t-map) and its applications to landmark matching registration. SIAM Journal on Imaging Sciences 7 (2014), 391–426. 3
- [LPD13] LIPMAN Y., PUENTE J., DAUBECHIES I.: Conformal Wasserstein distance: II. computational aspects and extensions. *Math. Comput.* 82, 281 (2013), 331–381. 3, 8
- [MR95] MASLEN D. K., ROCKMORE D. N.: Generalized FFTs a survey of some recent results. In *Proceedings of DIMACS Workshop in Groups* and Computation (1995), vol. 28, pp. 183–238. 3
- [PKC*16] PRADA F., KAZHDAN M., CHUANG M., COLLET A., HOPPE H.: Motion graphs for unstructured textured meshes. *ACM Trans. Graph.* 35, 4 (2016), 108:1–108:14. 1
- [Roc97] ROCKMORE D. N.: Some applications of generalized FFTs. In Proc. of DIMACS Workshop in Groups and Computation (1997), vol. 28, pp. 329–370. 3
- [Spr05] SPRINGBORN B. A.: A unique representation of polyhedral types. Centering via Möbius transformations. *Mathematische Zeitschrift* 249, 3 (2005), 513–517. 2
- [Spr18] SPRINGBORN B.:. personal communication, June 2018. 2
- [SSP08] SPRINGBORN B., SCHRÖDER P., PINKALL U.: Conformal equivalence of triangle meshes. ACM Transactions on Graphics (SIG-GRAPH '08) 27 (2008), 77:1–77:11. 1
- [SZS*13] SHI R., ZENG W., SU Z., WANG Y., DAMASIO H., LU Z., YAU S.-T., GU X.: Hyperbolic harmonic brain surface registration with curvature-based landmark matching. In *Information Processing in Medical Imaging* (2013), pp. 159–170. 3
- [ZS16] ZHANG H., SRA S.: First-order Methods for Geodesically Convex Optimization. arXiv e-prints (Feb. 2016). 2